PHYSICAL REVIEW B VOLUME 36, NUMBER 11 15 OCTOBER 1987-I

Vibrational properties of β_1-H and β_1-D on W(001): Electron-energy-loss measurements and lattice-dynamical calculations

J. P. Woods, A. D. Kulkarni, J. L. Erskine, and F. W. de Wette
Department of Physics, University of Texas, Austin, Texas 78712
(Received 13 February 1987)

High-resolution electron-energy-loss spectra are presented for β_1-H and β_1-D on W(001) for a variety of scattering geometries and scattering parameters. In addition to previously observed vibrational modes of this system corresponding to the symmetric stretch (130 meV), asymmetric stretch (160 meV), and wag (80 meV) modes, a new mode at 118 meV is observed and characterized. Angle-dependent studies of the vibrational peaks establish the dispersion of the hydrogen vibrational modes throughout the two-dimensional Brillouin zone. Lattice-dynamical calculations establish the origin of the 118-meV loss peak: It is found to be the optic version of the symmetric stretch mode, in which adjacent hydrogen atoms vibrate 180° out of phase.

I. INTRODUCTION

The chemisorption of hydrogen on tungsten surfaces is one of the most extensively studied systems in surface science. The tungsten surface is particularly interesting because of the variety of novel properties it exhibits.[1] Upon cooling below room temperature, surface atoms of clean W(001) displace along $\langle 110 \rangle$ directions forming alternating zigzag chains which yield a surface unit cell having $c(2\times2)$ symmetry, observed by low-energy electron diffraction (LEED).[2,3] This reconstruction can be viewed as the freezing in of the $\bar{M}_5$ phonon displacement. A saturated chemisorbed layer of hydrogen (β_1 phase) stabilizes the surface to (1×1) symmetry.[4,5] Extensive structural analysis based on LEED,[1-5] and MeV ion scattering,[6] as well as electron-energy-loss measurements,[7,8] have established the structural model for β_1-H on W(001), shown in Fig. 1; it is widely accepted and known as the Estrup-Anderson model. In this model there are two hydrogen atoms per surface unit cell, bridge bonded to the surface tungsten atoms.

A second ordered phase of hydrogen on W(001) exists at lower converges (β_2 phase). This phase is also characterized by a $c(2\times2)$ symmetry but with a different structure. The β_2 phase is accompanied by splitting and streaking of the LEED pattern as a function of additional hydrogen exposure until the (1×1) β_1 phase is formed.[4,5,9] Ion scattering experiments[6] have shown that the surface tungsten atoms are displaced laterally from their bulk positions and form surface dimers at low hydrogen coverage (β_2 phase). The hydrogen atoms are bridge bonded over surface dimer pairs. At saturation hydrogen coverage (β_1 phase), the surface tungsten atoms return to registry with the bulk lattice.

The vibrational properties of hydrogen on W(001) have been extensively investigated using electron-energy-loss spectroscopy (EELS).[7,8,10-12] In the simplest dynamical model, neighboring hydrogen atoms are assumed to be noninteracting, and based on the symmetry of both the β_1 and β_2 phases, three distinct vibrational modes of the adsorbed hydrogen atoms are expected to be observed. In the specific case of the β_1 phase, the three modes are illustrated in Fig. 1. The symmetric stretch (SS) mode corresponds to vibrational displacement perpendicular to the surface, the asymmetric stretch (AS) mode corresponds to displacement in the bridge plane in a direction parallel to the surface, and the wag mode corresponds to displacement perpendicular to the bridge plane. Based on symmetry, none of these modes are expected to be degenerate. Extensive EELS studies[7,8] of β_1-H and β_1-D on W(001) have established vibrational excitations associated with hydrogen at 80, 130, 160, and 260 meV. Original assignments of these excitation energies to the various modes are indicated in Fig. 1. The 260-meV excitation is double the energy of the symmetric stretch mode, and is thus assigned to an overtone of the 130-meV mode. The early experimental data on which the above assignments were made were obtained using energy resolution of approximately 30 meV full width at half maximum (FWHM).

Aers *et al.*[11] reported a full multiple-scattering calculation of the energy and angular dependence of the impact-scattering contribution to EELS spectra for β_1H/W(001). These results stimulated a detailed experimental examination of mechanisms responsible for electron energy losses from surface vibrations of β_1H/W(001) by Bare *et al.*[12] These experiments probed vibrational losses at large angles, both in and out of the incidence plane. In agreement with the earlier work,[8,9] these experiments revealed only a single electron loss at 130 meV in specular scattering geometry, while away from the specular direction, both in an out of the scattering plane, additional losses at 80 meV (wag mode) and 160 meV (asymmetric stretch mode) were observed. Large intensity variations of all three modes were observed in the backscattering directions and out of the incident plane, in general agreement with the theoretical predictions.[11]

More recently we have carried out additional investigations[10] of the vibrational properties of β_1H on W(001)

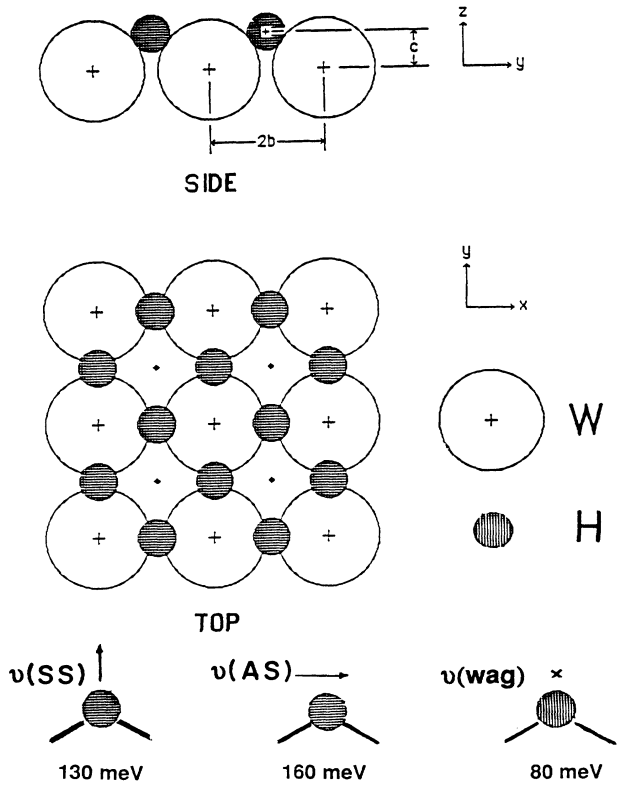

FIG. 1. Schematic representation of β_1H/W(001). The lattice constant of tungsten (3.16 Å) is taken as $2b$ for convenience, and the hydrogen atoms occupy bridge sites at a distance c above the tungsten surface. The radius of the tungsten atoms is scaled to its atomic radius of 1.37 Å, and the hydrogen atom radius is scaled to its Bohr radius of 0.53 Å. The crosses denote the center of the surface tungsten atoms, and the diamonds represent the center of the second layer tungsten atoms. Lower figures display the vibrational mode assignments for β_1H on W(001).

in an attempt to test certain predictions for large-angle-scattering selection rules.[13,14] Our EELS data were obtained at 7–10 meV energy resolution using a variety of scattering parameters including conditions under which LEED beams first emerge from the crystal surface. These studies revealed a new loss feature at 118 meV for β_1H on W(001). A corresponding vibrational signal at 83 meV was observed for β_1D on W(001), showing the loss feature to be an intrinsic hydrogen-adsorbate loss signal.

The incident energy and angle dependence of the 118-meV peak amplitude suggested that the mode associated with it is a parallel vibration, and this led us to suggest a new set of mode assignments for the β_1H vibrational structure.[10] The 130- and 80-meV mode assignments remained unchanged [namely, ν(SS)=130 meV, 2ν(SS) =260 meV, and ν(wag)=80 meV], but we reassigned ν(AS)=118 meV and 2ν(wag)=160 meV. Mode assignments for the β_2 phase[7] of H on W(001) are ν(SS)=155 meV, ν(AS)=120 meV, and ν(wag)=55 meV; i.e., ν(SS)>ν(AS)>ν(wag). In addition, previous investigators suggested the possibility that the 160-meV mode could be an overtone of the wag mode.

However there were difficulties with our initial assignment of the 118-meV feature to the asymmetric stretch mode. The height of adsorbed hydrogen atoms above the tungsten surface can be accurately estimated based on the vibrational properties of the adsorbed atoms. Assuming central-force interactions which yield simple harmonic motion, it can be shown that $\tan(\frac{1}{2}\alpha)=\nu(\mathrm{AS})/\nu(\mathrm{SS})$, where α is the angle subtended by the W-H-W bridge.[15] Using the bulk tungsten lattice constant (3.165 Å) and our new mode assignment ν(AS)=118 meV, the hydrogen-tungsten interlayer spacing (c) is estimated to be $c=1.74$ Å. The original mode assignment ν(AS)=160 meV yields $c=1.28$ Å. LEED I-V measurements[16] for β_1H on W(001) predict $c=1.17$ Å, and recent total-energy calculations of Weinert *et al.*[17] yield a value of $c=1.12$ Å. Similar calculations by Biswas and Hamann[18] yield $c=1.07$ Å. These results cast doubt on our initial assignment of the 118-meV loss peak to the asymmetric stretch mode. Also, several properties of the scattering behavior associated with this new mode (discussed later) suggest a re-evaluation of its origin.

Agrawal *et al.*[19] have carried out a lattice-dynamical calculation of the β_1H/W(001) system. Their model incorporates two-body as well as three-body interactions. The two-body interactions are considered up to the third hydrogen-tungsten neighbors, and nearest-neighbor hydrogen atoms. However, only the radial two-body forces are included. This model yields three distinct frequencies (instead of the four that we have observed) at the center of the two-dimensional surface Brillouin zone, and the symmetric stretch mode does not exhibit a $k_{\parallel}$ dependence (dispersion) across the two-dimensional Brillouin zone, as we have also observed.

In view of the above discussion, it now appears that the 160, 130, and 80 meV loss features of β_1H/W(001) are due to the asymmetric stretch, symmetric stretch, and wag modes, respectively, as originally assigned by Ho *et al.*[8] However, the 118-meV feature remains to be understood. In order to more fully understand the vibrational properties of β_1H/W(001), in particular the origin of the 118-meV mode, we have carried out additional experiments, and have investigated the lattice dynamical properties of this system in considerable detail.

The two-dimensional unit cell of β_1H/W(001) illustrated in Fig. 2 contains two hydrogen atoms, and therefore, in principle, there could be as many as six normal modes of hydrogen vibrations at each point in the two-dimensional Brillouin zone. In the noninteracting model which has been assumed to this point, three doubly degenerate modes are predicted, but the observation of four modes clearly suggests that hydrogen-hydrogen interactions are important. Using an exhaustive (16-parameter) model which incorporates two-body as well as three-body interactions, we are able to show that at most four distinct modes exist at the center of the two-dimensional Brillouin zone. These four modes are the three modes already described (symmetric stretch, asymmetric stretch, wag modes) and an "optic" mode involv-

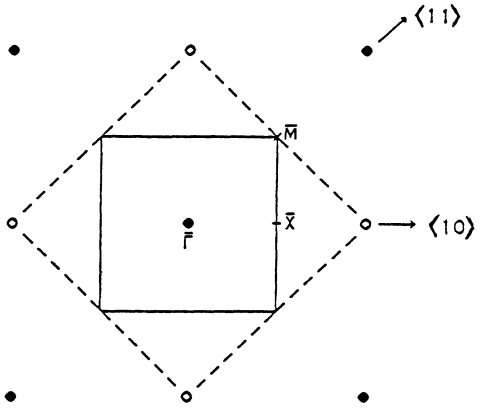

FIG. 2. Two-dimensional Brillouin zone (BZ) for β_1H/W(001) (solid lines), and that for the hydrogen sublattice (dotted lines). The reciprocal lattice of the hydrogen sublattice is denoted by filled circles. These points, together with the open circles constitute the reciprocal lattice of β_1H/W(001). The symmetry points of the BZ for β_1H/W(001) are also labeled. Note that the corners of the BZ of the hydrogen sublattice fold back onto the center ($\bar{\Gamma}$) of the BZ of β_1H/W(001).

ing *antiparallel* symmetric stretch motion of the two hydrogen atoms within a unit cell. The optic mode is a phonon at the corner of the Brillouin zone of the hydrogen sublattice, but occurs at the center ($\bar{\Gamma}$) of the Brillouin zone of β_1H/W(001), due to zone folding (see Fig. 2). Such coupled motion of hydrogen atoms also implies dispersion of the modes in the two-dimensional Brillouin zone, and the loss data and calculations presented here are consistent with a significant hydrogen-hydrogen interaction.

The symmetric stretch and optic modes are degenerate and dispersionless (i.e., are Einstein modes) in the absence of H-H interaction. We find that this degeneracy is lifted only in the presence of a nearest-neighbor H-H attraction or repulsion, or in the presence of a three-body H-H-W interaction. But the magnitude of the H-H-W interaction required to obtain the optic mode at 118 meV yields a very large dispersion in the wag mode, which is not observed in our experiments. This dispersion can be reduced only by an unphysical choice of parameters for the H-H-W interactions. On the other hand, a nearest-neighbor H-H repulsion correctly yields the optic mode below the symmetric-stretch-mode energy, and does not conflict with experimental data. The repulsion required to obtain the optic mode at 118 meV is an order of magnitude smaller than the first-neighbor H-W interaction. Thus our analysis leads in a natural way to a unique explanation of the nature of the 118 meV mode, and to the interaction responsible for it. It should be noted that our ordering of the symmetric stretch and optic modes disagrees with that calculated by Biswas and Hamann,[18] who find these modes to be at 141 and 150 meV, respectively; i.e., the optic mode lies *above* the symmetric stretch mode according to their calculation.

In Sec. II we discuss the experimental apparatus and procedures. In Sec. III we present EELS data at several incident energies and for several scattering geometries. In Sec. IV we present an extensive lattice-dynamical model of β_1H/W(001), and our interpretation of the origin of the 118-meV mode. A general discussion of our experimental results, model calculations, and our conclusions are presented in Sec. V.

II. EXPERIMENTAL DETAILS

Our experiments were performed using a modified Leybold-Heraeus ELS-22 spectrometer. Modifications of the lens system, described previously,[20] permit operation of the spectrometer at incident energies up to 300 eV. Additional modifications to the electronics permit[21] routine measurements of the elastic[22] and inelastic cross sections by simultaneously sweeping the monochromator exit-slit and analyzer entrance-slit voltages. This procedure results in a significant variation in spectrometer transmission function because the voltage on acceleration and deceleration optical elements are not varied. Therefore several sweeps at a sequence of initial kinetic energies are required to obtain intensity versus incident electron energy curves corresponding to elastic or inelastic scattering cross sections. The optics are tuned for maximum transmission at the center of each sweep increment.

The W(001) crystals were aligned with x-ray Laue techniques and spark cut or diamond-saw cut to within 1° of the (001) plane. The surface was polished with abrasive paper and 12-μm powder to a mirror finish. The (100) symmetry plane was identified with x-ray diffraction and was marked by spark cutting a shallow line on the back surface of the crystal. The crystals were cleaned by annealing at 1500–2100 °C in 10^{-7} torr oxygen for approximately 100 h and subsequent flashing to $\sim$2800 °C in ultrahigh vacuum in the 10^{-11} torr range. The tungsten crystals were mounted on two separate crystal manipulators for the several types of experiments reported in this paper. One manipulator provides access to the EELS optics along an axis perpendicular to the scattering plane. Samples mounted on this manipulator also had access to Auger analysis and Varian 4-grid LEED optics. A second manipulator enters the EELS scattering chamber in the scattering plane. Samples mounted on this manipulator can be rotated around the crystal normal direction. The combination of crystal azimuth rotation and angle-of-incidence changes permitted by the EELS optics provide access to a broad range of scattering configurations. The second manipulator provides access only to the EELS optics, however, the ability to operate the EELS optics at higher energies permits precise angular calibrations based on the observation of LEED beams.

III. EXPERIMENTAL RESULTS

Figure 3 displays EEL spectra for β_1H/W(001) for several incident energies ranging from 3.4 to 5.3 eV. These spectra were obtained using specular scattering geometry ($\theta_i = \theta_s = 60°$) with the crystal oriented to align

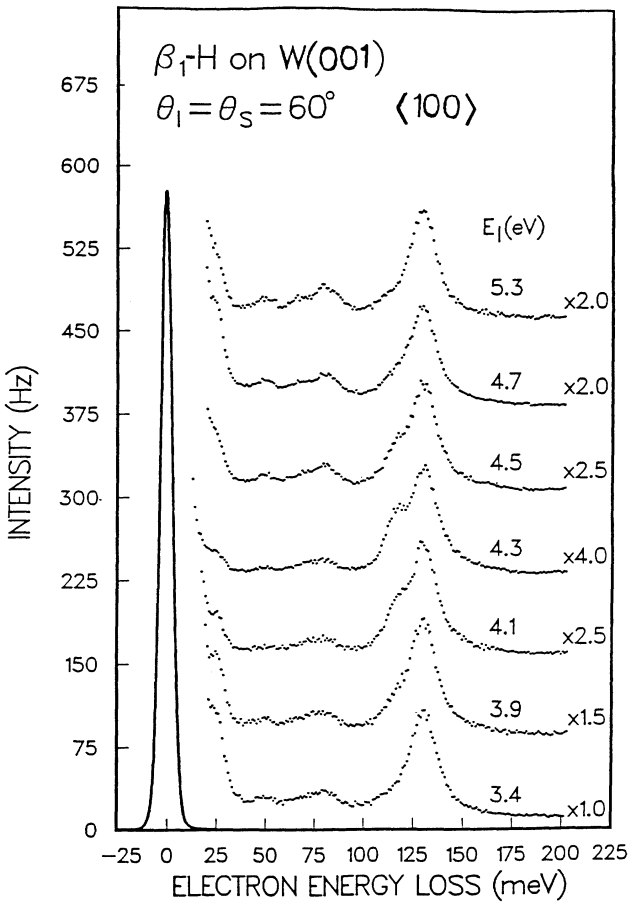

FIG. 3. Specular scattering EELS data for β_1 on W(001) at various incident energies around $E_i = 4.3$ eV. The scattering plane is along the (100) mirror plane. The baseline for each spectrum is shifted 75 Hz, and the loss spectra are magnified as indicated to the right of each spectrum.

the (100) crystal mirror plane along the scattering plane. The base line of each loss spectrum is shifted by 75 Hz. The numbers to the right of each loss spectrum indicate the scale factor used to plot data in the figure. The elastic peak indicates an energy resolution of 9 meV FWHM, and has been scaled to fit in the figure.

All spectra displayed in Fig. 3 clearly exhibit the symmetric-stretch-mode loss feature at 130 meV. The 80 meV wag mode is also apparent in all spectra with an intensity of approximately $\frac{1}{10}$ of the symmetric stretch mode. This observation is different from previous studies[7,8,12] of β_1H/W(001) in which the 80-meV mode was observed only in off-scattering geometry. At incident energies around $E_i = 4.3$ eV, an additional loss feature is clearly resolved at 118 meV. The scale factors show that at 4.3 eV, the 130-meV symmetric-stretch loss feature (cross section) is significantly decreased relative to the cross section probed at higher (5.3 eV) and lower (3.4 eV) incident energies.

The variation in elastic scattering cross section of the 130 meV loss peak can be understood on the basis of the scattering mechanism responsible for the loss signal. Symmetric stretch vibrations of the hydrogen atom produce dynamic dipole moments perpendicular to the surface (cf. Fig. 1). It is well established that long-range "dipole scattering" from dipole moments perpendicular to the surface dominate the inelastic loss signals measured by EELS[15] in specular-scattering geometry. The energy dependence of dipole-scattering cross sections is given by the product of a model-dependent factor (E_i^{-1} or E_i^{-2}) multiplied by the reflectance of the metal surface. Figure 4 displays the elastic reflectance of a clean W(001) surface and that of a β_1H/W(001) surface. Note that there is a minimum in reflectance at 4.3 eV for β_1H/W(001) when electrons are scattered at $\theta_i = 60°$ along the (100) plane. This minimum accounts for the suppression of the 130 meV loss peak evident in Fig. 3.

Figure 5 displays corresponding loss spectra for β_1D/W(001). In this series of spectra, the incident energy is held fixed at $E_i = 4.2$ eV, and the exit angle at which the loss feature was measured is held fixed at $\theta_s = 60°$. As in Fig. 4, the scattering plane is along the ⟨100⟩ crystal direction. The incident angle θ_i is varied in this case, and the spectra are plotted as a function of $k_\parallel$, the momentum transfer parallel to the ⟨100⟩ direction. At $k_\parallel = 0$, corresponding to $\theta_i = \theta_s = 60°$, three

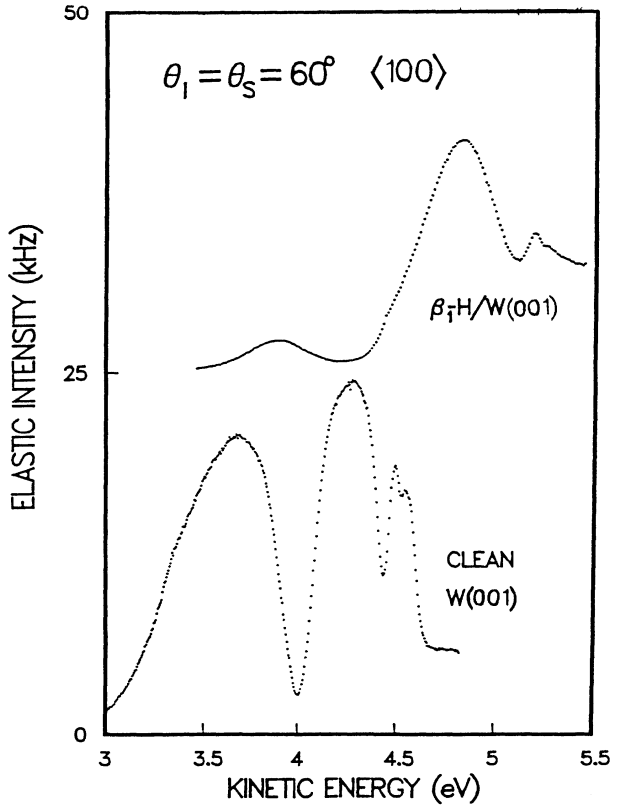

FIG. 4. Very low energy electron reflectance intensity vs acceleration voltage $I(V)$ curves for clean W(001), and for β_1H on W(001). The scattering plane is aligned with the (100) mirror plane of the surface. The baseline of the β_1H on W(001) curve is shifted 25 kHz.

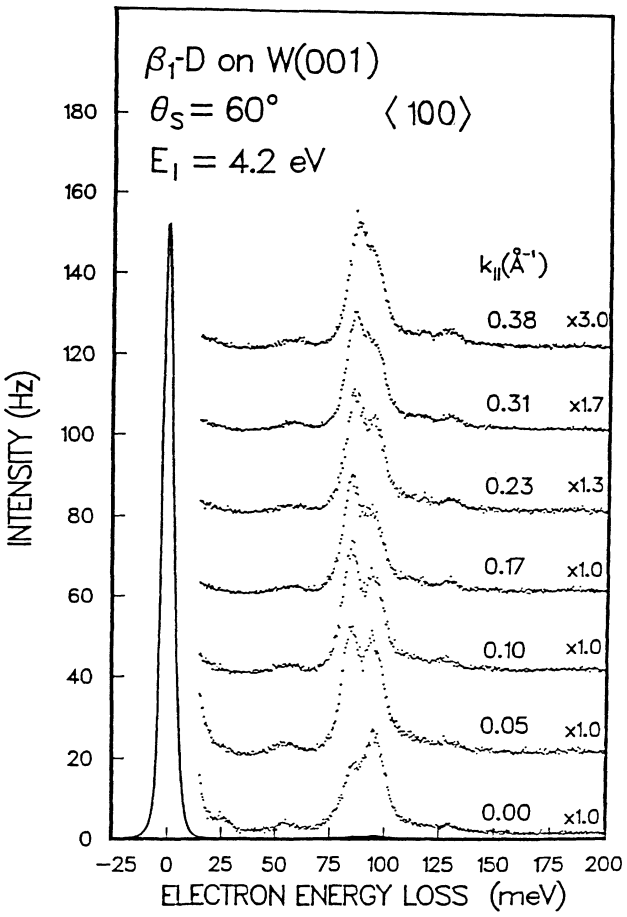

FIG. 5. Specular ($k_{\parallel}=0$) and off-specular EELS data for β_1D on W(001) at an electron kinetic energy of 4.2 eV. The scattering plane is along the (100) mirror plane of the surface. Off-specular geometry is obtained by rotating the monochromator toward the crystal normal with the scattered angle fixed at $\theta_s=60°$. The monochromator is rotated 5° between successive loss spectra, and the distance across the surface Brillouin zone is indicated in the figure. Baselines are shifted 20 Hz and magnifications are indicated to the right of each spectrum.

modes at 92, 83, and 55 meV are apparent in the spectra. These peaks are the 130, 118, and 80 meV hydrogen loss peaks shifted down by $\sqrt{2}$, the mass ratio. The relative peak intensities of the 92 and 83 meV peaks at $k_{\parallel}=0$ are similar to the corresponding 130 and 118 meV loss peaks for hydrogen at the same incident energy (cf. spectra in Figs. 3 and 5). The relative cross sections of the 92 and 83 meV modes change as a function of θ_i [or $k_{\parallel}=(2m/\hbar)\sqrt{E_i}\sin\theta$] as illustrated by the spectra in Fig. 5. The 92-meV mode cross section decreases significantly for nonspecular angles. (Scale factors are again shown to the right of the spectra.) This behavior is expected on the basis of the predominantly dipole nature of the scattering from the symmetric stretch mode. The observed angle dependence of loss peaks corresponding to the 92 and 83 meV modes suggest that the 83 meV (deuterium) and 118 meV (hydrogen) peaks are produced predominantly by a scattering mechanism which is not dipole in nature.

This conclusion may seem to contradict our interpretation of the 118-meV mode as the "optic" mode (described in the Introduction). In the optic mode, hydrogen atoms vibrate perpendicular to the tungsten surface, and therefore one might expect dipole scattering to be the dominant scattering mechanism. However, in this mode the displacements of nearest-neighbor hydrogen atoms are 180° out of phase. Hence the *dynamical* dipole moments of the hydrogen atoms cancel each other in the far-field region where dipole scattering occurs, and therefore an incoming electron does not experience any dipole field, until it comes very close to a hydrogen atom. Then it can be scattered only by the impact-scattering mechanism.

Close inspection of the loss peaks reveals that the vibrational energies disperse with $k_{\parallel}$ throughout the two-dimensional Brillouin zone. This variation of vibrational energies as a function of $k_{\parallel}$ is a clear indication of coupling between adjacent hydrogen atoms. Figure 6

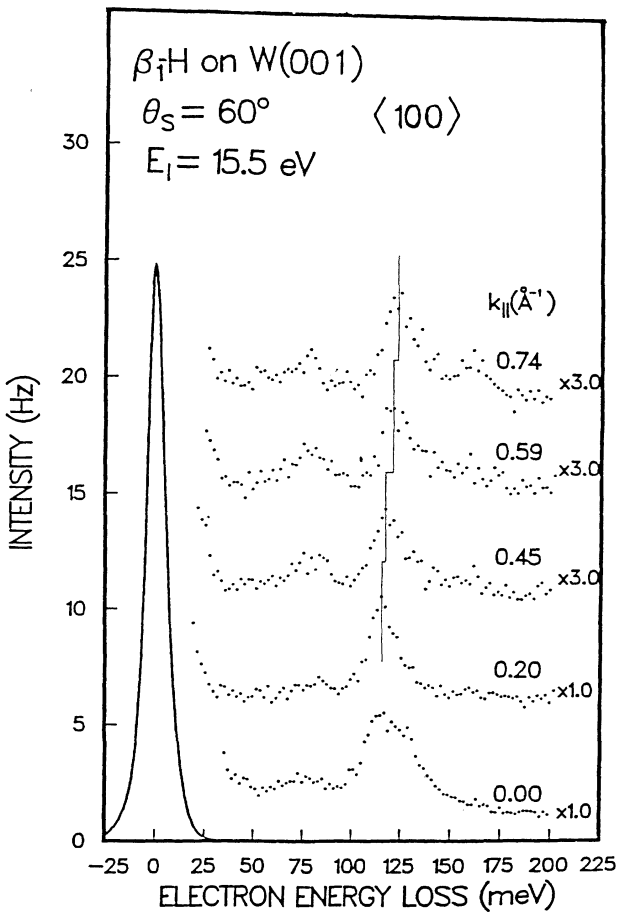

FIG. 6. Specular ($k_{\parallel}=0$) and off-specular EELS data for β_1H on W(001) at electron kinetic energy of 15.5 eV. The scattering plane is along the (100) mirror plane of the surface. Distances across the surface Brillouin zone are indicated for each spectrum. Baselines are shifted 5 Hz and the magnification of each spectrum is shown at the right of each spectrum.

displays the $k_\parallel$ dependence of EELS spectra for β_1H/W(001), obtained for scattering along the (100) crystal plane. A relatively high incident energy was chosen ($E_i = 15.5$ eV) to suppress contributions of the 130 meV loss resulting from the symmetric stretch mode. Note that under these scattering conditions at $k_\parallel = 0$ (specular-scattering geometry), the 118 meV loss peak is significantly stronger than the 130 meV loss peak. As the incident angle is varied away from $\theta_i = 60°$, the small dipole contribution at 130 meV from the symmetric stretch mode rapidly disappears, and it is possible to determine the dispersion ($k_\parallel$ dependence) of the 118-meV mode. The energy resolution is 10 meV, and due to the separation between the 118 and 130 meV loss features and the relative amplitudes of these peaks, it is clear that the peak shift is real and not a consequence of a relative amplitude change in the two adjacent loss peaks.

The dispersion of the 118 meV loss peak versus $k_\parallel$, shown in Fig. 6, is determined to be 7±3 meV along the $\bar{\Gamma}\bar{X}$ line of the two-dimensional Brillouin zone. This dispersion was determined by the displacement of the peak of Gaussian fits to the experimental data as $k_\parallel$ was varied. At an incident energy $E_i = 15.5$ eV, $\Delta k_\parallel = 0.20$ Å^{-1} corresponds approximately to $\Delta\theta = 10°$. Since the dipole-scattering angular profile varies approximately as $\hbar\omega_{\text{loss}}/E_{\text{inc}}$, it is not surprising that the dipole contribution from the 130 meV loss is not observed for $\theta \neq 0$. The spectra for $k_\parallel = 0.74$ Å^{-1} also clearly exhibit the two parallel vibrational losses at 80 and 160 meV which result from the wag and asymmetric stretch modes. The signal-to-noise ratio of data in Fig. 6 is not sufficiently good to obtain the dispersion of these modes.

As described in the previous section, one of our manipulators permits accurate and continuous rotation of the crystal about the crystal normal while in the EELS scattering position. Figure 7 displays EELS data for β_1H/W(001), obtained using specular-scattering geometry at $E_i = 14.7$ eV as a function of azimuthal-angle setting of the manipulator. A value of $\phi_{\text{man}} = 337°$ corresponds to scattering in the (100) mirror plane of the crystal. This figure illustrates the sensitivity of the 118 meV mode cross section to scattering-plane orientation. The strongest scattering occurs for scattering along the (100) mirror planes. There are apparent nulls in the cross section of the 118 meV mode along the (110) mirror planes. This observation is discussed in more detail later.

Figure 8 displays selected loss spectra for β_1H and β_1D on W(001) obtained for specular scattering along the ⟨110⟩ direction. Spectra for three incident energies are displayed for the hydrogen-covered surface; one spectrum is shown for deuterium coverage. Reflectance curves (not shown) similar to those displayed in Fig. 4 reveal a deep minimum in the electron elastic reflectance at $E_i = 4.7$ eV at $\theta_i = 60°$ with the plane of incidence along the ⟨110⟩ azimuth. Under these scattering conditions, all three of the principal vibrational modes (at 80, 130, and 160 meV) are clearly resolved in specular scattering geometry (upper three curves). The corresponding modes, shifted down in energy by $\sqrt{2}$, are

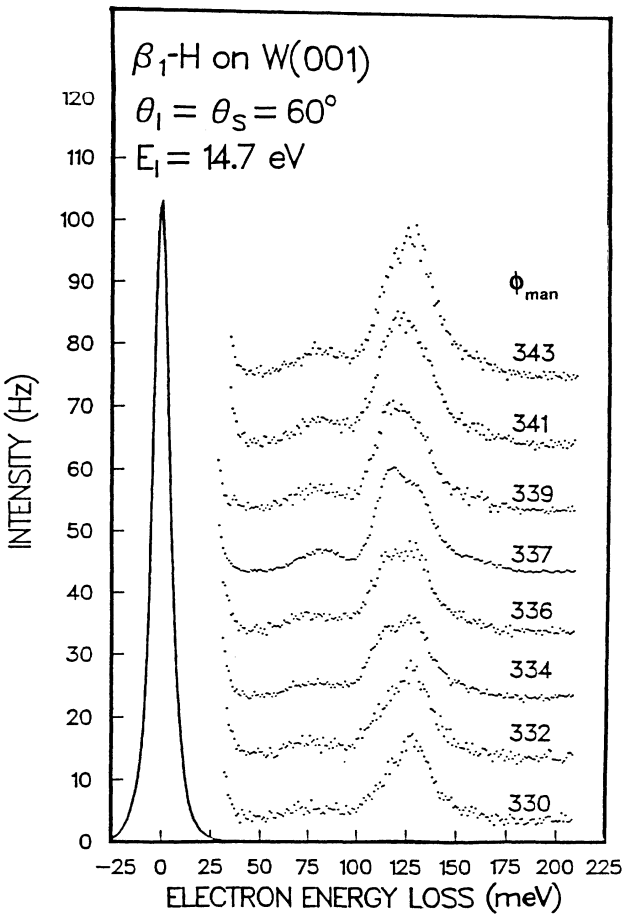

FIG. 7. Specular EELS data for β_1H on W(001) for various orientations of the scattering plane along the crystal surface. Electron incident energy is 14.7 eV. The ϕ values indicated in the plot are the values from the crystal manipulator. The value $\phi = 337$ was established as the (100) mirror plane by a groove on the crystal to an accuracy of ±2°. All spectra are ×1, and the baselines are shifted by 10 Hz.

shown for β_1D (lower spectrum). The main point of Fig. 8 is that the 118 meV is *not* observed in spectra taken along the ⟨110⟩ azimuth.

Figure 9 displays specular and off-specular EELS data for the scattering plane along the (110) mirror plane at a higher impact energy. The resolution has been reduced because of low counting rates. The 80- and 160-meV modes are observed in off-specular geometry, and it is clear that the 160 meV cross section does not increase at the same rate as the 80 meV cross section. The 160 meV cross section is larger at $k_\parallel = 0.43$ and 0.73 Å^{-1} than it is at 1.01 Å^{-1}, while the 80 meV cross section increases steadily as the parallel momentum is increased. The 160-meV mode does not appear to be an overtone or a double loss of the 80 meV mode because of the observed intensity ratio. There is a slight dispersion in the wag mode (at 80 meV), but higher resolution experiments will be needed to accurately measure it. The features near 130 meV do not show the dominance of the 118-meV

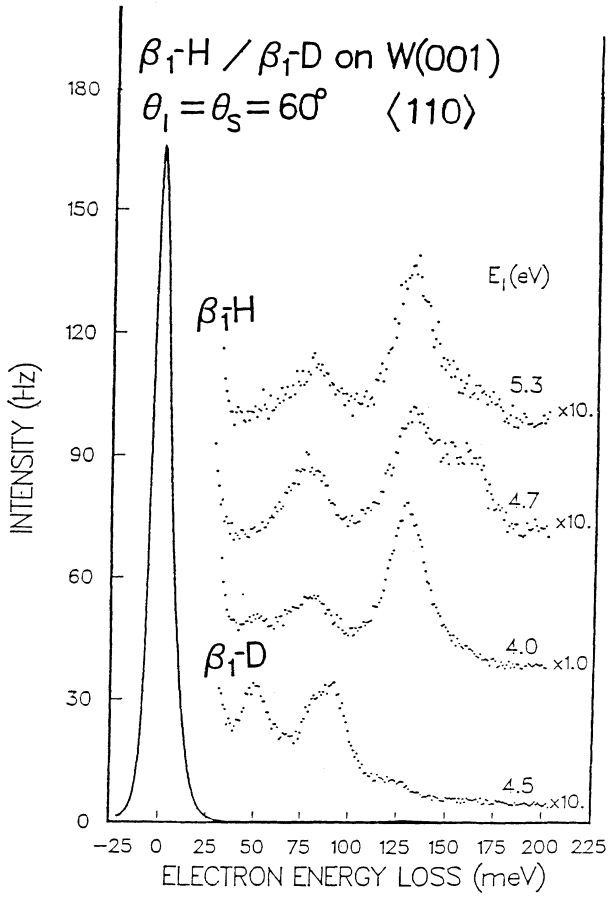

FIG. 8. Specular EELS data for β_1H and β_1D on W(001) at various kinetic energies with the scattering plane aligned with the (110) mirror plane. Baselines are shifted by 30 Hz, and the number to the right of each spectrum is the magnification used in displaying the EELS.

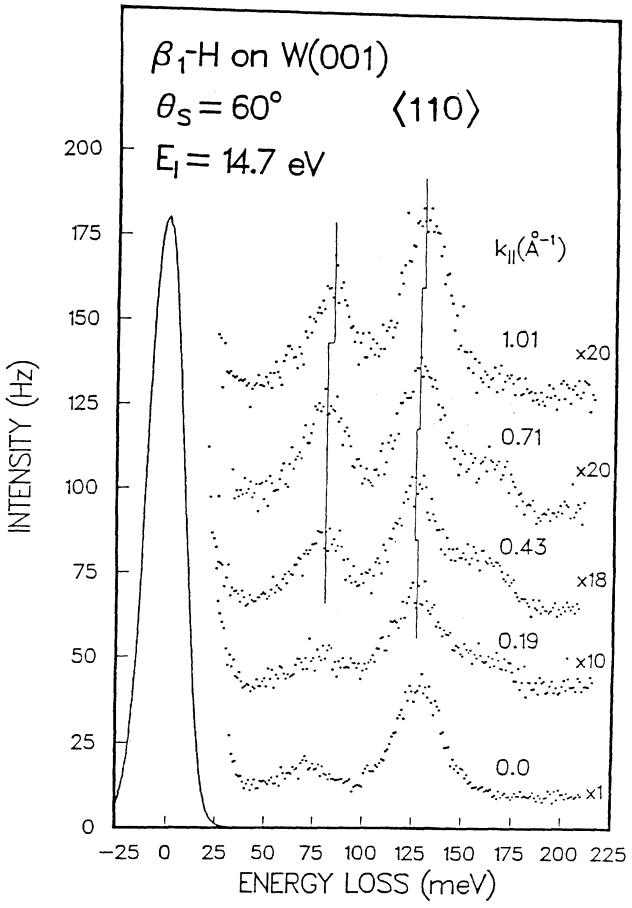

FIG. 9. Specular ($k_{\parallel}=0$) and off-specular EELS data for β_1H on W(001) at incident electron kinetic energy of 14.7 eV, and with the scattering plane aligned with the (110) mirror plane. Baselines are shifted 25 Hz and the magnification used to display the loss spectra are indicated to the right of the spectra. The distance across the surface Brillouin zone is indicated for each spectrum.

mode as was observed in Fig. 6.

Summarizing the experimental results presented in this section: Four vibrational modes have been observed for β_1H and β_1D on W(001). All modes exhibit the expected $\sqrt{2}$ decrease in frequency when deuterium is substituted for hydrogen; otherwise the loss data are identical or very similar. The 118-meV hydrogen (83-meV deuterium) mode is observed in specular scattering geometry along the (100) crystal plane at specific energies where the symmetric stretch dipole cross section is suppressed by reflectance effects. The 118-meV mode can be observed in off-specular scattering geometry when the other parallel modes at 80 and 160 meV are also observed. The 118-meV mode does not appear to be observed in spectra obtained for $k_{\parallel}$ along the (110) crystal plane. High energy resolution angle-dependent spectra exhibit dispersion of the hydrogen-induced loss peak energies as a function of $k_{\parallel}$ in the two-dimensional Brillouin zone, suggesting coupled motion of the hydrogen atoms. These observations are now examined in view of a lattice dynamical model for β_1H/W(001).

IV. DYNAMICS OF β_1H/W(001)

A. Description of the model

The configuration of β_1H/W(001) is described in the Introduction and is shown in Fig. 1. For later convenience, we denote the lattice constant of the tungsten lattice by $2b$, and the perpendicular distance between the hydrogen atoms and the top tungsten layer by c. We use the following terminology to avoid awkward constructions: By "nth-neighbor H-H," we mean an nth-neighbor hydrogen atom of a given H, and by "nth-neighbor H-W," we mean an nth-neighbor tungsten atom of a given H.

In our model of β_1H/W(001), we include all H-H two-body interactions up to the second neighbor H-H's, and all H-W two-body interactions up to the third-neighbor H-W's, as shown in Fig. 10. W1 in Fig. 10 denotes the first-neighbor H-W interaction; similarly for W2, W3, and H1. As the second-neighbor H-H's occur

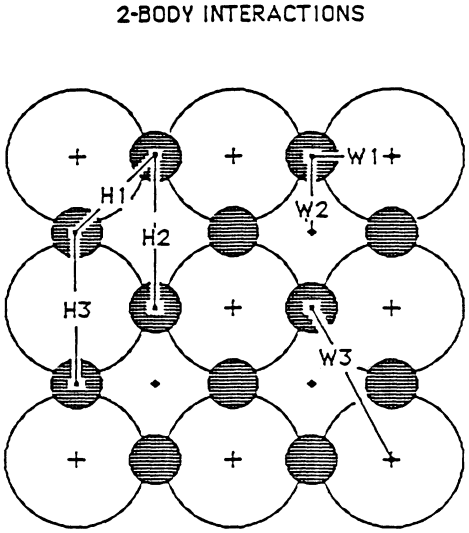

FIG. 10. The two-body interactions considered in the lattice dynamical model. There are two types of second-neighbor H-H pairs, and they are denoted differently as H2 and H3.

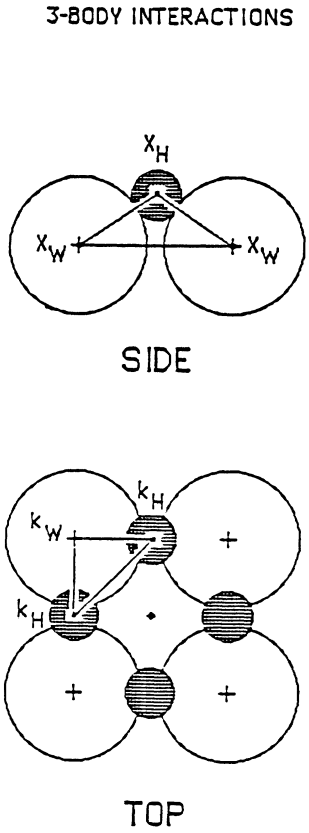

FIG. 11. The three-body interactions considered in the lattice dynamical model. The H-W-W and H-H-W triangles and the corresponding interaction parameters are shown.

in two distinct configurations, we denote the corresponding interactions differently, by H2 and H3. The H-W interactions are included up to the third-neighbors, since the third-neighbor H-W bond-length is comparable to the second-neighbor H-H bond-length, due to the large radius (1.37 Å) of the tungsten atoms, and due to the geometry of the bridge-bond over the bcc lattice. We also include H-H-W and H-W-W three-body interactions, where H-H and H-W are first neighbors (Fig. 11).

We assume that the two-body interactions can be described by central potentials $\phi(r)$, where r is the separation of the two particles. In the lattice dynamical problem, we need only the first two derivatives of ϕ, which we denote by

$$\alpha=\phi''(R) \quad \text{and} \quad \beta=R^{-1}\phi'(R) , \tag{1}$$

where R is the equilibrium separation. Then the first-neighbor H-W interactions are given by the parameters α_{W1} and β_{W1}. Similarly, W2, . . . , H3 yield $\alpha_{W2}, \ldots, \beta_{H3}$.

We model the three-body interactions in terms of angle-bending forces as follows: Given three particles A,B,C, they constitute a triangle with an angle, say θ, at A. We associated a "stiffness constant" k_{ABC} with this angle, which gives rise to the potential

$$\tfrac{1}{2}k_{ABC}(\theta-\theta_0)^2 , \tag{2}$$

where θ_0 is the equilibrium value of θ. Similarly, there are stiffness constants k_{BCA} and k_{CAB} associated with the angles at B and C. In the β_1H/W(001) problem, due to symmetry, this model gives rise to stiffness constants k_H, k_W, and χ_H, χ_W, for the triplets H-H-W and H-W-W discussed above (see Fig. 11). In this way, the total number of parameters in our model becomes 16.

In Sec. IV B we present the eigenvalue problem for hydrogen vibrations in the frozen-substrate approximation and obtain analytical expressions for the eigenvalues. Having analytical expressions greatly facilitates our study of the modes of hydrogen—especially their dependence on the interaction parameters. We have also carried out these calculations numerically by the slab method.[23] We find that the error in the frequencies given by the analytical expressions, due to the frozen substrate approximation is less than 0.3%.

B. Vibrational modes of hydrogen

The two-dimensional primitive cell of β_1H/W(001) has translation vectors $(2b,0)$ and $(0,2b)$ (see Fig. 1), and in the frozen substrate approximation, has a basis of two hydrogen atoms, which we denote by u and v. u is at $(b,0,c)$ and v is at $(0,b,c)$. When these atoms are displaced from their equilibrium positions by $\mathbf{u}$, $\mathbf{v}$, and those associated with the lattice points $(2b,0)l_1 + (0,2b)l_2$ (l_1,l_2 integers) are displaced by $(\mathbf{u},\mathbf{v})\exp i2b(q_1l_1+q_2l_2)$, we find the restoring forces $\mathbf{F}_u$, $\mathbf{F}_v$ on u,v to be given by

$$\begin{bmatrix} F_{uz} \\ F_{vz} \\ F_{ux} \\ F_{vx} \\ F_{uy} \\ F_{vy} \end{bmatrix} = - \begin{bmatrix} Z+z_1 & h & 0 & p & 0 & t \\ h^* & Z+z_2 & r & 0 & s & 0 \\ 0 & r^* & X+x_1 & e & 0 & f \\ p^* & 0 & e^* & Y+y_1 & g & 0 \\ 0 & s^* & 0 & g^* & Y+y_2 & e \\ t^* & 0 & f^* & 0 & e^* & X+x_2 \end{bmatrix} \begin{bmatrix} u_z \\ v_z \\ u_x \\ v_x \\ u_y \\ v_y \end{bmatrix} , \tag{3}$$

where

$$Z = K_z + 4\beta_{H1} + \gamma_W + \gamma_H ,$$
$$X = K_x + 2(\alpha_{H1} + \beta_{H1}) + (c^4\gamma_W + b^4\gamma_H)(bc)^{-2} ,$$
$$Y = K_y + 2(\alpha_{H1} + \beta_{H1}) + \gamma_W(b^2+c^2)^2(bc)^{-2} ,$$
$$z_1 = 4\beta_{H3}\sin^2(bq_1) + 4\beta_{H2}\sin^2(bq_2) ,$$
$$z_2 = 4\beta_{H2}\sin^2(bq_1) + 4\beta_{H3}\sin^2(bq_2) ,$$
$$x_1 = 4\alpha_{H3}\sin^2(bq_1) + 4\beta_{H2}\sin^2(bq_2) ,$$
$$x_2 = 4\beta_{H2}\sin^2(bq_1) + 4\alpha_{H3}\sin^2(bq_2) ,$$
$$y_1 = 4\alpha_{H2}\sin^2(bq_1) + 4\beta_{H3}\sin^2(bq_2) ,$$
$$y_2 = 4\beta_{H3}\sin^2(bq_1) + 4\alpha_{H2}\sin^2(bq_2) ,$$
$$h = (-4\beta_{H1} + \gamma_W - \gamma_H)e^{ib(q_1-q_2)}\cos(bq_1)\cos(bq_2) ,$$
$$e = -[2(\alpha_{H1} + \beta_{H1}) + \gamma_W(b^2+c^2)b^{-2}]e^{ib(q_1-q_2)}\cos(bq_1)\cos(bq_2) ,$$
$$f = [2(\alpha_{H1} - \beta_{H1}) + (c^4\gamma_W - b^4\gamma^H)(bc)^{-2}]e^{ib(q_1-q_2)}\sin(bq_1)\sin(bq_2) ,$$
$$g = [2(\alpha_{H1} - \beta_{H1}) + \gamma_W(b^2+c^2)^2(bc)^{-2}]e^{-ib(q_1-q_2)}\sin(bq_1)\sin(bq_2) ,$$
$$p = -i\gamma_W(b^2+c^2)(bc)^{-1}e^{ib(q_1-q_2)}\sin(bq_1)\cos(bq_2) ,$$
$$t = -i(c^2\gamma_W + b^2\gamma_H)(bc)^{-1}e^{ib(q_1-q_2)}\cos(bq_1)\sin(bq_2) ,$$
$$r = -i(c^2\gamma_W + b^2\gamma_H)(bc)^{-1}e^{-ib(q_1-q_2)}\sin(bq_1)\cos(bq_2) ,$$
$$s = -i\gamma_W(b^2+c^2)(bc)^{-1}e^{-ib(q_1-q_2)}\cos(bq_1)\sin(bq_2) .$$

In these expressions we have used

$$\gamma_H = \frac{2c^2(b^2+2c^2)}{b^2(b^2+c^2)^2}k_H , \tag{4}$$
$$\gamma_W = \frac{2b^2c^2}{(b^2+2c^2)(b^2+c^2)^2}(2k_W + k_H) , \tag{5}$$
$$K_x = \frac{2b^2}{b^2+c^2}(\alpha_{W1} - \beta_{W1}) + \frac{4b^2}{5b^2+c^2}(\alpha_{W3} - \beta_{W3}) + 2(\beta_{W1} + \beta_{W2} + \beta_{W3}) + \frac{2c^2}{(b^2+c^2)^2}\chi_W , \tag{6}$$
$$K_y = \frac{2b^2}{b^2+(b+c)^2}(\alpha_{W2} - \beta_{W2}) + \frac{16b^2}{5b^2+c^2}(\alpha_{W3} - \beta_{W3}) + 2(\beta_{W1} + \beta_{W2} + 2\beta_{W3}) , \tag{7}$$
$$K_z = \frac{2c^2}{b^2+c^2}(\alpha_{W1} - \beta_{W1}) + \frac{2(b+c)^2}{b^2+(b+c)^2}(\alpha_{W2} - \beta_{W2}) + \frac{4c^2}{5b^2+c^2}(\alpha_{W3} - \beta_{W3}) + 2(\beta_{W1} + \beta_{W2} + 2\beta_{W3}) + \frac{4b^2}{(b^2+c^2)^2}\chi_H + \frac{2b^2}{(b^2+c^2)^2}\chi_W . \tag{8}$$

Note that in K_x, K_y, K_z, we have grouped together all H-W interaction terms which do not give any dispersion to the hydrogen modes.

The dynamical matrix $\underline{D}$ in this problem is just the 6×6 matrix in Eq. (3), and its eigenvalues $m\omega^2$ (m is the mass of the hydrogen atom) yield the normal modes of the hydrogen sublattice. At the zone center, i.e., at $(q_1,q_2)=(0,0)$, all terms in $\underline{D}$ except X, Y, Z, h, and e vanish. Then $\underline{D}$ becomes block diagonal, and has eigenvalues

$$\lambda_z = Z \pm h \ ,$$
$$\lambda_{x,y} = \tfrac{1}{2}(X+Y) \pm \tfrac{1}{2}[(X-Y)^2 + 4\,|\,e\,|^2]^{1/2} \ ,$$

where $\lambda_{x,y}$ are doubly degenerate. Also, here h and e are understood to be evaluated at $(q_1,q_2)=(0,0)$. Thus in this model, there are at most four distinct modes at the zone center.

As the H-W interactions are expected to be much stronger than the H-H interactions, from $\lambda_{x,y}$ we find that the asymmetric stretch (AS) and the wag modes have eigenvalues

$$\lambda(\mathrm{AS}) = X + O\left[\frac{|\,e\,|^2}{(X-Y)^2}\right] ,$$
$$\lambda(\mathrm{wag}) = Y + O\left[\frac{|\,e\,|^2}{(X-Y)^2}\right] , \tag{9}$$

where the assignments of these modes are obtained from their eigenvectors. Similarly from λ_z, the eigenvalues of the symmetric stretch (SS) and optic modes are found to be

$$\lambda(\mathrm{SS}) = Z + h \equiv Z - 4\beta_{\mathrm{H1}} + \gamma_{\mathrm{W}} - \gamma_{\mathrm{H}} \ ,$$
$$\lambda(\mathrm{optic}) = Z - h \equiv Z + 4\beta_{\mathrm{H1}} - \gamma_{\mathrm{W}} + \gamma_{\mathrm{H}} \ . \tag{10}$$

Since it is established[8,18] that the 160-, 130-, and 80-meV modes are the asymmetric stretch, symmetric stretch, and wag modes, respectively, we conclude that the 118-meV mode is the optic mode. This assignment is also supported by the dispersion data and the exhibited symmetries of scattering cross section, as we will show below.

From Eqs. (10) it is clear that only the nearest neighbor H-H interaction β_{H1}, and the H-H-W three-body interactions make the optic mode different in frequency from the symmetric stretch mode. In order to determine which of these interactions is significant, we examine the dispersion of all modes within our model.

In order to determine the eigenvalues at arbitrary (q_1,q_2), we first note that only X,Y,Z in the dynamical matrix contain K_x,K_y,K_z, in which all H-W interactions are grouped together. Since the H-W interactions are expected to be much stronger than the H-H interactions, X,Y,Z are much larger than the other entries in $\underline{D}$ (which are written in the lower case for that reason). We therefore calculate the eigenvalues at arbitrary (q_1,q_2) by treating the lower case entries as perturbations to the diagonal matrix with diagonal elements (Z,Z,X,Y,Y,X).

The perturbational approach, in addition to being simpler, also makes the dependence of the eigenvalues on the interaction parameters more transparent. We shall see the eigenvalues accurate up to the first order will be adequate for our purpose. To calculate the first-order corrections, we expand $\det(\underline{D}-\lambda\underline{I})$ up to the second order in the lower case quantities

$$\begin{aligned}\det(\underline{D}-\lambda\underline{I}) = {} & (Z+z_1-\lambda)(Z+z_2-\lambda)(X+x_1-\lambda)(X+x_2-\lambda)(Y+y_1-\lambda)(Y+y_2-\lambda) \\ & - |\,h\,|^2(X-\lambda)^2(Y-\lambda^2) - (Z-\lambda)^2[\,|\,f\,|^2(Y-\lambda)^2 + |\,g\,|^2(X-\lambda)^2 - 2\,|\,e\,|^2(X-\lambda)(Y-\lambda)] \\ & - (Z-\lambda)(X-\lambda)(Y-\lambda)[(\,|\,p\,|^2 + |\,s\,|^2)(X-\lambda) + (\,|\,r\,|^2 + |\,t\,|^2)(Y-\lambda)] \ . \end{aligned} \tag{11}$$

The first term on the right-hand side of (11) is not expanded to keep the expression simple. The third- and fourth-order terms in this expression are to be ignored. Now note that the eigenvalues of the unperturbed dynamical matrix are X,Y,Z. The first-order correction to these eigenvalues can be obtained as follows: Set $\lambda = Z + \delta\lambda_z$ in (11). Then to the second order,

$$\det[\underline{D} - (Z+\delta\lambda_z)\underline{I}] = [(z_1-\delta\lambda_z)(z_2-\delta\lambda_z) - |\,h\,|^2] \times (X-Z)^2(Y-Z)^2 \ ,$$

from which the first-order corrections to $\lambda = Z$ are seen to be

$$\delta\lambda_z = \tfrac{1}{2}(z_1+z_2) \pm \tfrac{1}{2}[(z_1+z_2)^2 + 4\,|\,h\,|^2]^{1/2} \ . \tag{12}$$

A similar procedure yields the following first-order corrections to $\lambda = X$ and $\lambda = Y$:

$$\delta\lambda_x = \tfrac{1}{2}(x_1+x_2) \pm \tfrac{1}{2}[(x_1+x_2)^2 + 4\,|\,f\,|^2]^{1/2} \ , \tag{13}$$

$$\delta\lambda_y = \tfrac{1}{2}(y_1+y_2) \pm \tfrac{1}{2}[(y_2+y_2)^2 + 4\,|\,g\,|^2]^{1/2} \ . \tag{14}$$

Thus the eigenvalues at arbitrary (q_1,q_2) accurate up to the first order are $X+\delta\lambda_x$, $Y+\delta\lambda_y$, $Z+\delta\lambda_z$, where $\delta\lambda_x$, $\delta\lambda_y$, $\delta\lambda_z$, are as given above. Some of the parameters in these expressions are constrained by the requirements that at $\bar{\Gamma}=(0,0)$, the asymmetric stretch, symmetric stretch, optic, and wag modes be at 160, 130, 118, and 80 meV, respectively. That is, from Eqs. (9) and (10) we find

$$\begin{aligned} \lambda(\mathrm{AS}) &= X = (160\ \mathrm{meV})^2 \ , \\ \lambda(\mathrm{wag}) &= Y = (80\ \mathrm{meV})^2 \ , \\ \lambda(\mathrm{SS}) &= Z + h = (130\ \mathrm{meV})^2 \ , \\ \lambda(\mathrm{optic}) &= Z - h = (118\ \mathrm{mev})^2 \ , \end{aligned} \tag{15}$$

which implies

$$Z=(124\ \text{meV})^2\ ,$$

and

$$h\equiv -4\beta_{\text{H1}}+\gamma_{\text{W}}-\gamma_{\text{H}}=(38.6\ \text{meV})^2\ . \tag{16}$$

We now use these values to calculate the dispersion of the normal modes along the $\bar{\Gamma}\bar{X}$ and $\bar{\Gamma}\bar{M}$ directions (Fig. 2). To facilitate a comparison of these dispersions with experiments, we first plot in Fig. 12, the dispersion data for hydrogen modes, obtained from Figs. 6 and 9. Next we calculate the eigenvalues at $\bar{X}=(\pi/2b)(1,0)$. They are given by

$$\lambda(\text{optic})=Z=(124\ \text{meV})^2\ ,$$

$$\lambda(\text{SS})=Z+z_1+z_2\ ,$$

$$\lambda(\text{AS})=X \quad \text{and} \quad X+x_1+x_2\ ,$$

$$\lambda(\text{wag})=Y \quad \text{and} \quad Y+y_1+y_2\ ,$$

where z_1+z_2, x_1+x_2, and y_1+y_2 are understood to be evaluated at $\bar{X}$. Thus we see that the asymmetric stretch and wag modes become nondegenerate at $\bar{X}$ and have small dispersions of x_1+x_2 and y_1+y_2, respectively. [The dispersions are small since x_i, y_i, z_i $(i=1,2)$ are much smaller than X, Y, Z.] This result is consistent with our experiments (see Fig. 6), where there is no noticeable dispersion in the asymmetric stretch and wag modes.

According to the above equations, along $\bar{\Gamma}\bar{X}$, the optic mode increases from 118 to 124 meV, and the symmetric stretch mode decreases from 130 meV to $124+(z_1+z_2)/248$ meV. That is, at $\bar{X}$, the symmetric stretch and optic modes are separated by a small gap of $(z_1+z_2)/248$ meV. An upward shift in the energy of the 118-meV mode is indeed observed in our experiments (see Figs. 6 and 12), confirming its assignment as the optic mode. But we do not have any dispersion data along $\bar{\Gamma}\bar{X}$ for the symmetric stretch mode, since in the off-specular geometry, its cross section becomes very small compared to that of the optic mode. We have plotted the theoretical dispersions obtained above in Fig. 12 and they appear to be consistent with the experimental data. In calculating these dispersions we have set $x_i,y_i,z_i=0$ $(i=1,2)$, since we do not have enough data to estimate these parameters. Hence in Fig. 12 the symmetric stretch and optic modes at $\bar{X}$ are seen to be degenerate $(=124$ meV).

It was pointed out in the Introduction, that the symmetric stretch and optic modes lie at the center and corner, respectively, of the Brillouin zone of the hydrogen sublattice (dashed square in Fig. 2). Since both modes involve vibrations perpendicular to the W(001) surface, they lie on the *same* dispersion curve in the Brillouin zone of the hydrogen sublattice. Thus in the Brillouin zone of β_1H/W(001), the dispersion of symmetric stretch and optic modes along $\bar{\Gamma}\bar{X}$ arises from the folding of a single dispersion curve. This explains our finding that along $\bar{\Gamma}\bar{X}$, the symmetric stretch and optic modes disperse towards each other (Fig. 12).

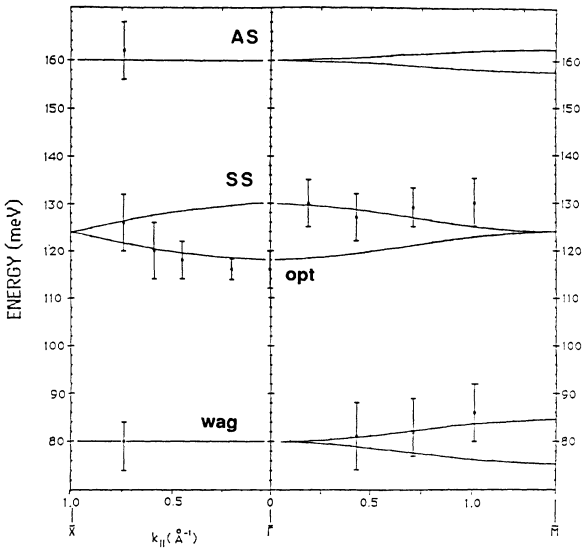

FIG. 12. Calculated and measured dispersion of the hydrogen vibrational modes of β_1H on W(001) across high symmetry directions of the W(001) surface Brillouin zone.

Next we calculate the normal mode dispersions along $\bar{\Gamma}\bar{M}$. Setting $x_i,y_i,z_i=0$ $(i=1,2)$ we find that the eigenvalues at $\bar{M}=\pi/2b(1,1)$ are given by

$$\begin{aligned}
&\lambda(\text{optic})=\lambda(\text{SS})=Z=(124\ \text{meV})^2\ ,\\
&\lambda(\text{AS})=X\pm|f|\\
&\qquad=X\pm[2(\alpha_{\text{H1}}-\beta_{\text{H1}})\\
&\qquad\quad+(c^4\gamma_{\text{W}}-b^4\gamma_{\text{H}})(bc)^{-2}]\ ,\\
&\lambda(\text{wag})=Y\pm|g|\\
&\qquad=Y\pm[2(\alpha_{\text{H1}}-\beta_{\text{H1}})\\
&\qquad\quad+\gamma_{\text{W}}(b^2+c^2)^2(bc)^{-2}]\ .
\end{aligned} \tag{17}$$

The theoretical dispersion of the optic and symmetric stretch modes along $\bar{\Gamma}\bar{M}$ is similar to that along $\bar{\Gamma}\bar{X}$ (Fig. 12). The dispersion curve of the symmetric-stretch mode is seen to be consistent with the experimental data. We do not observe the optic mode in this direction, whereas the wag mode can be observed and has a small dispersion (Fig. 9). We use the latter fact to decide as to which interaction in h (H-H or H-H-W) is significant in the occurrence of the optic mode.

Note from (17) that the dispersion of the asymmetric stretch and wag modes depends on α_{H1}, β_{H1}, γ_{W}, and γ_{H}, which must satisfy the relation

$$h\equiv -4\beta_{\text{H1}}+\gamma_{\text{W}}-\gamma_{\text{H}}=(38.6\ \text{meV})^2=1488\ \text{meV}^2\ , \tag{18}$$

obtained earlier. Suppose the H-H-W interaction is significant. Then we set $\alpha_{\text{H1}}=\beta_{\text{H1}}=0$ in (18) and (17), and obtain

$$\lambda(\text{wag})=Y\pm(\gamma_{\text{W}}-\gamma_{\text{H}}+\gamma_{\text{H}})[(b^2+c^2)/(bc)]^2\ .$$

Taking $2b=3.165$ Å and $c=1.11$ Å, we find

$$\lambda(\text{wag})=6400\pm4.525(1488+\gamma_H)$$
$$=6400\pm(6733+4.525\gamma_H)\ \text{meV}^2\ ,$$

which is a very large dispersion, unless $\gamma_H\approx-1488$ meV^2. In order to estimate γ_H, we assume that the dispersion in the wag mode is ±10 meV (which is a very conservative estimate in view of Figs. 9 and 12). For this dispersion, we find $\gamma_H=-1112$ meV^2 and $\gamma_W=375.7$ meV^2. Substituting these value in Eqs. (4) and (5) we obtain $k_W=-1.16k_H$; i.e., the stiffness of the angle at W is comparable in magnitude with the stiffness of the angles at H, which is unphysical. Hence the H-H-W interaction cannot be a mechanism for the occurrence and dispersion of the optic mode.

Now let us examine the other possibility. With $\gamma_H=\gamma_W=0$, from Eq. (18) we get $\beta_{H1}=-372$ meV^2. The negative value of β_{H1} means that the nearest-neighbor hydrogen atoms repel each other. However, compared to the H-W interactions, which typically are $\sim\frac{1}{2}(130\ \text{meV})^2=8450$ meV^2, this repulsion is exceedingly weak. With $\beta_{H1}=-372$ meV^2, the wag mode becomes

$$\lambda(\text{wag})=6400\pm(744+2\alpha_{H1})\ \text{meV}^2\ . \quad (19)$$

For a realistic dispersion of ±6 meV in the wag mode (see Fig. 12), we obtain $\alpha_{H1}=110$ meV^2. With these parameters, the dispersion in the asymmetric stretch mode becomes ±3 meV.

It may seem that this model is also not quite satisfactory since the parameters α,β in force constant models are normally related by $|\alpha|\approx10|\beta|$. In contrast to this we have $|\alpha_{H1}|<|\beta_{H1}|$. However, it should be noted that the relation $|\alpha|\approx10|\beta|$ is established by considering the dominant forces in these models, whereas the configuration of the hydrogen sublattice is mainly governed by the H-W interactions, and the H-H forces are of secondary important. Consequently, the violation of this relation is not necessarily a drawback of the model. Thus we conclude that this model is valid and that the optic mode arises due to a repulsive interaction between the nearest-neighbor hydrogen atoms.

V. DISCUSSION

In this paper we have studied, experimentally as well as theoretically, the vibrational modes of hydrogen adsorbed on the (001) surface of tungsten, with saturated hydrogen coverage [i.e., the β_1H/W(001) phase]. The experimental investigation was carried out using electron energy loss spectroscopy. We measured loss spectra using several tungsten crystals, with an energy resolution of ~10 meV. In addition to the loss features of 160, 130, and 80 meV reported earlier,[7,8,12] we consistently observed a fourth loss feature at 118 meV.

We have also studied the dispersion of several loss features of β_1H/W(001) along the $\bar{\Gamma}\bar{X}$ and $\bar{\Gamma}\bar{M}$ directions of the two-dimensional Brillouin zone. Along $\bar{\Gamma}\bar{X}$, the 118 meV mode disperses upward, and the 160 and 80 meV modes do not have any noticeable dispersion (Figs. 6 and 12). The dispersion of the 130 meV mode cannot be observed in this direction, as its cross section diminishes considerably in off-specular geometry, and thereby it is masked by the 118 meV mode. Along $\bar{\Gamma}\bar{M}$, corresponding to the $\langle110\rangle$ crystal direction, due to smaller cross sections, our data were obtained at lower resolution than along $\bar{\Gamma}\bar{X}$. (The spectra in Fig. 9 are magnified by a factor of 20 relative to those in other figures.) We do not observe the 118-meV mode in this direction. The 80- and 160-meV modes (parallel vibrations) are observed in off-specular scattering geometry along the $\langle110\rangle$ direction. The 80-meV mode has a small dispersion, but higher resolution experiments are required to measure it accurately.

In previous EELS studies of β_1H/W(001), loss features at 160, 130, and 80 meV have been identified as being due to the asymmetric stretch, symmetric stretch, and wag modes, respectively.[7,8] Our additional experiments and the lattice dynamical model presented here offer a reasonable explanation of the new 118-meV mode that we have observed. Our strategy was to view the substrate-adsorbate unit cell as a coupled dynamical system and to set up an extensive interaction model to describe the dynamical properties of this system.

We find that even with the inclusion of all 16 parameters in our model, there are at most four distinct modes at the zone center, namely the asymmetric stretch, symmetric stretch, wag, and the "optic" modes. Thus we associate the 118 meV loss feature with the optic mode, in which nearest-neighbor hydrogen atoms vibrate 180° out of phase, with displacements perpendicular to the surface. This mode occurs at the corner of the Brillouin zone of the hydrogen sublattice, but is observed at the center ($\bar{\Gamma}$) of the Brillouin zone of β_1H/W(001), due to zone folding (Fig. 2). The relative cross sections along $\bar{\Gamma}\bar{X}$, of the 92 and 83 meV loss peaks for deuterium (Fig. 5) suggest that the 83 meV (deuterium) and 118 meV (hydrogen) peaks arise due to the impact scattering mechanism. This conclusion is consistent with our interpretation of the 118-meV mode as the optic mode. To see this, note that although hydrogen atoms vibrate perpendicular to the tungsten surface in the optic mode, the displacements of nearest-neighbor hydrogen atoms are 180° out of phase. Consequently, the far-field *dynamical* dipole moments of adjacent hydrogen atoms cancel each other, and an incoming electron does not see a long-range dipole field. Therefore the optic mode can scatter only by the impact scattering mechanism.

The frequency of the optic mode is predicted to shift from 118 to 124 meV for wave vectors along $\bar{\Gamma}\bar{X}$ and $\bar{\Gamma}\bar{M}$ directions. This shift is observed along the $\bar{\Gamma}\bar{X}$ direction in our experiments. We do not detect the 118-meV mode along the $\bar{\Gamma}\bar{M}$ direction (see Figs. 8 and 9), which in fact supports our assignment of this mode as the optic mode. Since the scattering plane along $\langle110\rangle$ is a mirror plane in the symmetry group C_{4v} of β_1H/W(001), and that the optic mode is *odd* with respect to this mirror plane, it follows that the impact scattering cross section must vanish in this scattering geometry.[14] It is interesting to note that the impact scattering selection rules are not required to explain the absence of scattering intensity along the $\langle110\rangle$ direction. The two

out-of-phase dipoles within the unit cell constitute an effective quadrupole, the field of which has a nodal plane along the (110) scattering plane. For completeness, we also mention that our ordering of the symmetric stretch and optic modes disagrees with that obtained by Biswas and Hamann[18] from total energy calculations. These authors find that the optic mode lies *above* the symmetric stretch mode.

According to our model, the symmetric stretch mode should disperse from 130 to 124 meV along the $\bar{\Gamma}\bar{X}$ and $\bar{\Gamma}\bar{M}$ directions (Fig. 12). In the experiments, along $\bar{\Gamma}\bar{X}$, the symmetric stretch mode is dominated by the optic mode, and thus cannot be observed. However, along the $\bar{\Gamma}\bar{M}$ direction, the optic mode is not seen, and we do observe dispersion in the symmetric stretch mode as predicted by our model. The model predicts no dispersion for the asymmetric stretch and the wag modes along $\bar{\Gamma}\bar{X}$, and the experimental data are consistent with this prediction. Along $\bar{\Gamma}\bar{M}$, the asymmetric stretch and wag modes are predicted to become nondegenerate (see Fig. 12), and are expected to have dispersions of ~ 3 and ~ 6 meV, respectively. The noise in our data makes it difficult to accurately determine the dispersion of the asymmetric stretch mode. However the predicted dispersion of the wag mode appears to be in agreement with the experimental data. The nondegeneracy of this mode cannot be verified due to the poor resolution in our data along the $\bar{\Gamma}\bar{M}$ direction.

The optic and symmetric stretch modes have different frequencies either as a result of the nearest-neighbor H-H interaction, or as a result of the H-H-W three-body interaction. The latter interaction is ruled out since it requires an unphysical choice of interaction parameters. On the other hand, a weak nearest-neighbor repulsion correctly yields the optic mode at 118 meV. Thus our analysis leads to the conclusion that the 118-meV mode is the optic mode, and that the mode arises due to a weak repulsion of nearest-neighbor hydrogen atoms.

ACKNOWLEDGMENTS

This work was sponsored by grants from AFOSR (AFOSR-86-0109), NSF (DMR-8505747), and the Robert A. Welch Foundation (F-433 and F-1015).

[1]A. J. Melmed and W. R. Graham, Appl. Surf. Sci. **11/12**, 470 (1982).
[2]T. E. Felter, R. A. Barker, and P. J. Estrup, Phys. Rev. Lett. **38**, 1138 (1977).
[3]M. K. Debe and D. A. King, Phys. Rev. Lett. **39**, 708 (1977); J. Phys. C **10**, L303 (1977).
[4]R. A. Barker and P. J. Estrup, Phys. Rev. Lett. **41**, 1307 (1978); J. Chem. Phys. **74**, 1442 (1981).
[5]D. A. King and G. Thomas, Surf. Sci. **92**, 201 (1980).
[6]I. Stensgaard, L. C. Feldman, and P. J. Silverman, Phys. Rev. Lett. **42**, 247 (1979).
[7]M. R. Barnes and R. F. Willis, Phys. Rev. Lett. **41**, 1729 (1978).
[8]W. Ho, R. F. Willis, and E. W. Plummer, Phys. Rev. Lett. **40**, 1463 (1978); Phys. Rev. B **21**, 4202 (1980).
[9]P. J. Estrup and J. Anderson, J. Chem. Phys. **45**, 2254 (1966).
[10]J. P. Woods and J. L. Erskine, Phys. Rev. Lett. **55**, 2595 (1985).
[11]G. Aers, J. B. Pendry, T. B. Grimley, and K. L. Sebastian, J. Phys. C **14**, 3995 (1981).
[12]S. R. Bare, P. Hofmann, M. Surman, and D. A. King, J. Electron Spectrosc. Relat. Phenom. **29**, 265 (1983).
[13]B. M. Hall, S. Y. Tong, and D. L. Mills, Phys. Rev. Lett. **50**, 1277 (1983).
[14]S. Y. Tong, C. H. Li, and D. L. Mills, Phys. Rev. B **24**, 806 (1981).
[15]H. Ibach and D. L. Mills, *Electron Energy Loss Spectroscopy and Surface Vibrations* (Academic, New York, 1982).
[16]M. A. Passler, B. W. Lee, and A. Ignatiev, Surf. Sci. **150**, 263 (1985).
[17]M. Weinert, A. J. Freeman, and S. Ohnishi, Phys. Rev. Lett. **56**, 2295 (1986).
[18]R. Biswas and D. R. Hamann, Phys. Rev. Lett. **56**, 2291 (1986).
[19]B. K. Agrawal, B. Djafari-Rouhani, and L. Dobrzynski, Surf. Sci. **89**, 446 (1979); B. K. Agrawal, Phys. Rev. B **22**, 3734 (1980).
[20]R. L. Strong and J. L. Erskine, Rev. Sci. Instrum. **55**, 1304 (1984); Phys. Rev. B **31**, 6305 (1985).
[21]J. P. Woods, Ph.D. Dissertation, The University of Texas at Austin, 1986.
[22]J. P. Woods and J. L. Erskine, J. Vac. Sci. Technol. (to be published).
[23]R. E. Allen, G. P. Alldredge, and F. W. de Wette, Phys. Rev. B **4**, 1648 (1971).